Sodium Dodecyl Sulfate−Polyacrylamide Gel Electrophoresis and Förster Resonance Energy Transfer Suggest Weak Interactions between Fibroblast Growth Factor Receptor 3 (FGFR3) Transmembrane Domains in the Absence of Extracellular Domains and Ligands†

Edwin Li,‡ Min You,‡ and Kalina Hristova*

Department of Materials Science and Engineering, Johns Hopkins University, Baltimore, Maryland 21218

Received July 16, 2004; Revised Manuscript Received October 19, 2004

ABSTRACT: Lateral dimerization of membrane proteins has evolved as a means of signal transduction across the plasma membrane for all receptor tyrosine kinases (RTKs). The transmembrane (TM) domains of RTKs are proposed to play an important role in the dimerization process. We have investigated whether the TM domains of one RTK, fibroblast growth factor receptor 3 (FGFR3), dimerize in lipid vesicles in the absence of the extracellular domains and ligands. We have performed sodium dodecyl sulfate−polyacrylamide gel electrophoresis (SDS−PAGE) with peptides produced via solid-phase peptide synthesis that correspond to the TM domain of FGFR3. We have carried out Förster resonance energy transfer (FRET) measurements using two donor−acceptor pairs, fluorescein/rhodamine and Cy3/Cy5, as a function of peptide concentration and donor-to-acceptor mole ratios. Our results suggest that FGFR3 TM domains form sequence-specific dimers in lipid bilayers. However, the dimerization propensity of FGFR3 TM domain is much weaker than the dimerization propensity of glycophorin A (GpA), the well-characterized "membrane dimer standard". We discuss our findings in the context of cell signaling across the plasma membrane and diseases or disorders that occur due to single amino acid mutations in the TM domain of FGFR3.

Receptor tyrosine kinases (RTKs)[1] conduct biochemical signals via lateral dimerization in the plasma membrane. They play a key role in the regulation of various cellular processes, such as control of cell growth and differentiation. Different RTKs have been implicated in developmental abnormalities (*1*) and diseases, including some cancers (for instance, mammary and ovary carcinomas) (*2*), gliomas, psoriasis, restenosis, and pulmonary fibrosis (*3*).

RTKs are type I transmembrane proteins with their N-termini outside the cell and single TM domains. The extracellular (ligand-binding) domains, usually several hundred amino acids long, contain characteristic arrays of structural motifs. The TM domain is followed by a juxtamembrane region and a catalytic domain, which is about 250 amino acid residues long and related to that of soluble tyrosine kinases.

RTKs are believed to exist in a monomer−dimer equilibrium. In signal transduction, a ligand (a growth factor) binds to the receptor and stabilizes the dimeric state by inducing conformational change in the extracellular domain (*4*). As a result, the two cytoplasmic domains come into contact. The contact stimulates catalytic activity and results in the intermolecular autophosphorylation of the receptor subunits. This activates the catalytic domains for the phosphorylation of cytoplasmic substrates and triggers signaling cascades.

While the extracellular domains of RTKs play a crucial role in ligand recognition and dimerization (*5*−*7*), a question remains as to the role of the TM domains in the dimerization process. This is a controversial issue: the TM domains may be merely passive anchors (*8*), or they may be the driving force for dimerization (*9*).

The TM domains seem to be important for the dimerization of at least some RTKs, as suggested by the finding that a single amino acid substitution in the TM domain can lead to constitutive receptor activation and therefore to pathologies (*1*, *10*−*14*). Furthermore, substitutions that are analogous to these mutations have been engineered in related RTKs and have been shown to be activating (*10*, *15*). Recently, the four TM domains of the human epidermal growth family receptors, ErbB, have been shown to dimerize in the absence of the extracellular domains or ligands in bacterial membranes (*16*).

In this paper, we assess the dimerization propensity of the TM domains of fibroblast growth factor receptor 3 (FGFR3) in model systems and calculate the free energy of dimerization. FGFR3 is a receptor tyrosine kinase that consists of an extracellular domain with three immunoglobulin-like motifs, a single TM domain, and an intracellular split tyrosine

† This work was supported by NIH Grant GM068619 to K.H.

* To whom correspondence should be addressed. E-mail: kh@jhu.edu. Tel: 410-516-8939. Fax: 410-516-5293.

‡ Contributed equally to this work.

[1] Abbreviations: TM, transmembrane; RTK, receptor tyrosine kinase; FGFR3, fibroblast growth factor receptor 3; Fl, fluorescein; Rhod, rhodamine; POPC, 1-palmitoyl-2-oleoyl-*sn*-glycero-3-phosphocholine; HFIP, hexafluoroisopropanol; GpA, glycophorin A; NBD-PE, *N*-(7-nitrobenz-2-oxa-1m3-diazol-4-yl)-1,2-dihexadecanoyl-*sn*-glycero-3-phosphoethanolamine.

10.1021/bi048480k CCC: $30.25
Published on Web 12/09/2004

kinase domain. FGFR3 plays a key role in the development of the skeletal system, and mutations in its TM domain have been identified as genetic causes of skeletal dysplasias and craniofacial syndromes (*17*). Examples include the achodroplasia-causing Gly380→Arg, the Ala391→Glu mutation, which causes Crouzon syndrome with acanthosis nigricans, and Gly370→Cys, Ser371→Cys, and Tyr373→Cys, causing thanatophoric (lethal) dysplasia. It has been proposed that these mutations cause unregulated signaling by stabilizing the mutant dimers (*18*).

Using sodium dodecyl sulfate−polyacrylamide gel electrophoresis (SDS−PAGE) and Förster resonance energy transfer (FRET) measurements in liposomes, we find that FGFR3 TM domains can dimerize in the absence of extracellular domains and ligands. However, the dimerization is relatively weak, having free energy of dimerization of about −3 kcal/mol. These results provide a starting point for understanding the thermodynamic consequences of the pathogenic mutations in the FGFR3 TM domain and the effect of lipid composition on the interactions between RTK TM domains.

MATERIALS AND METHODS

FGFR3 TM Domain. The FGFR3 TM domain, amino acid sequence DEAGSVYAGILSYGVGFFLFILVVAAVTLCRLR, was custom synthesized at the Kansas State Biotechnology Facility. The peptides were purified using reverse-phase HPLC and water/acetonitrile gradient. Correct molecular weight of 3520.2 Da was confirmed using matrix-assisted laser desorption ionization time of flight (MALDI-TOF) mass spectrometry. The single cysteine residue in the protein was labeled with either Cy3−maleimide/Cy5−maleimide (Amersham) or fluorescein−maleimide/tetramethylrhodamine−maleimide (Molecular Probes). The dyes were attached to Cys396, a naturally occurring cysteine in the TM domain of FGFR3. Cys396 is close to the C-terminus of the peptide and is expected to be outside of the helical membrane-embedded domain of the peptide. CD spectra show that the helicity of the peptides never exceeds ∼25 000 deg cm^2/dmol, corresponding to ∼70% helicity (as seen in Figures 2 and 3), suggesting that the termini of the peptide, containing the charges, are disordered. We therefore expect that the dyes will be free to rotate in space such that the measured FRET will depend only on the distance between donors and acceptors.

For the labeling reaction, approximately 2 mg of protein was dissolved in 400 μL of HFIP and 800 μL of 10 mM phosphate buffer at pH 7. The dyes were first dissolved in 50 μL of methanol (MeOH) and then mixed with the protein. The reaction was carried out at room temperature with frequent mixing for the first 30 min and then left in the refrigerator overnight. Excess dye was removed using a C2 solid-phase extraction column (Varian). The labeled proteins were further purified by HPLC (Varian).

A challenge in HPLC purification of the labeled peptide arose because the labels did not increase substantially the hydrophobicity of the already very hydrophobic peptides. As a result, the labeled and unlabeled peptides eluted at the same time from the HPLC column and could not be separated. We found that we could achieve high labeling yields with Fl/Rhod (between 80% and 100% labeling yields), while labeling yields for the bulkier Cy3/Cy5 were typically between 30% and 70%. Percent labeling was determined from the ratio of peptide concentrations (as measured by CD) to the label concentration (measured by absorbance). To determine the free energy of dimerization, the FRET efficiency due to dimerization was calculated by subtracting calculated FRET efficiency due to proximity from the measured FRET efficiency and then correcting the result for incomplete labeling (if needed). Corrections due to proximity FRET are discussed in detail in the Results section. Corrections due to incomplete labeling were applied to dimerization-induced FRET in Figure 10 as follows: Let us assume 90% labeling for both donor and acceptor. The maximum FRET for completely labeled, all-dimeric peptides is 50%. The maximum FRET for 90% labeled all-dimeric peptides is calculated as 45%. Therefore, a correction of 50/45 = 1.125 is applied to the dimerization-induced FRET efficiency. It should be noted that data corresponding to peptide labeling <90% were not used in the free energy calculation in Figure 10 such that the applied corrections were small.

Circular Dichroism. CD spectra of FGFR3 TM domain in HFIP/water, SDS, and lipid vesicles were collected using a Jasco 710 spectropolarimeter. The concentrations of the peptides in the samples, required for calculating molar ellipticities, were determined from absorbance measurements in a Cary 50 (Varian) spectrophotometer.

The CD measurements have demonstrated that the peptides are always helical if dissolved in HFIP first. During sample preparation, we always dissolved the peptides in HFIP first and then added other solvents as needed.

Oriented CD. Oriented CD measurements were performed as previously reported (*19*−*22*). Peptides and lipids were codissolved in HFIP/chloroform. Dropwise, the solution was deposited on a quartz slide, and the solvent was removed under a stream of nitrogen to form a multilamellar sample containing the peptides. The quartz slide was mounted on a custom-designed chamber. To hydrate, a drop of water was placed in the chamber, and the sample was equilibrated for several hours. The chamber was placed in the Jasco 710 spectropolarimeter such that the multilayers were perpendicular to the beam. The sample was rotated around the beam axis in increments of 45°. Eight discreet spectra were thus collected and averaged.

SDS−PAGE. The peptide samples were subjected to SDS−PAGE using 10−20% tricine precast gels (Novex, San Diego, CA). The TM domains were dissolved in SDS-containing sample buffer, reduced with NuPAGE reducing agent, sometimes boiled for 5 min, and loaded onto the gels. Boiling did not affect the results. The peptides were visualized with Coomassie blue. The dimer−monomer ratios were calculated using the public domain NIH ImageJ software.

Preparation of Vesicles. 1-Palmitoyl-2-oleoyl-*sn*-glycero-3-phosphocholine (POPC) was purchased from Avanti. Lipids and proteins were first mixed in HFIP/chloroform. Solvents were removed under a stream of nitrogen gas; the mixture was lyophilized and then redissolved in 10 mM phosphate buffer, 500 mM NaCl, pH 7. Samples were then freeze−thawed several times, which substantially decreased the turbidity of the samples. Some FRET measurements were performed in such liposomal systems. In some cases, Triton

X-100 was added to the lipid samples below its CMC, at a ratio of one detergent molecule to seven lipids (the exact amount of Triton incorporated into the liposomes is not known). Triton addition further decreased the turbidity of the samples such that now we could not only measure the FRET efficiencies but also obtain a CD spectrum and confirm that the peptides are helical (see Figure 3, dotted line). Alternatively, the liposomal samples were extruded using a 100 nm pore diameter membrane (Avanti) to produce large unilamellar vesicles (LUVs). The final concentration of the proteins in the LUV solutions was determined from absorbance measurements using a Cary UV/vis spectrophotometer (Varian).

In all cases, FRET was measured before and after extrusion or detergent addition. Typically we observed a slight decrease, by 2−5%, in measured FRET efficiencies after extrusion or detergent addition. This slight decrease may be explained by eliminating the possibility of FRET occurring between donor and acceptor in different bilayers in the multilamellar samples. Although the exact mechanism is unknown, the observed decrease is less than our typical experimental errors, and we consider this change negligible.

Therefore, the FRET efficiency measured in unextruded liposomes, extruded liposomes, and detergent-doped unextruded liposomes is the same. However, a high-quality CD spectrum can be collected only for extruded liposomes and detergent-doped unextruded liposomes.

Sample Homogeneity. When peptides and lipids are mixed in organic solvents, they can either (1) form a homogeneous mixture, that is, a single "phase", or (2) segregate into two or more distinct lipid-rich and peptide-rich phases. The FRET method heavily relies on the assumption that the two components can be completely and thoroughly mixed to form a single phase. We therefore assessed homogeneity of peptide/lipid mixtures using X-ray diffraction, fluorescence microscopy, and FRET efficiencies as described below.

In X-ray studies of multilamellar liposomes, a homogeneous sample gives rise to a single set of Bragg peaks. A phase-separated sample shows either (1) two sets of Bragg peaks or (2) a single set of Bragg peaks, identical to pure lipid samples, and one or several sharp lines due to protein aggregates. We carried out X-ray scattering experiments with "dry" (i.e., ambient humidity) protein/lipid mixtures. The intensity-versus-2Θ data for dry protein/lipid mixtures always exhibited a single set of Bragg peaks (data not shown), and the relative intensities of the peaks differed from intensities recorded for pure DOPC. These experiments therefore suggest that the proteins and lipids are thoroughly mixed and form a single phase.

Furthermore, we observed no macroscopic phase separation in surface-supported bilayers containing the TM domains. Vesicles containing Cy3-labeled TM domains and NBD-PE were incubated with clean microscope slides to form single surface-supported bilayers and were imaged in a Nikon 600 fluorescence microscope. The fluorescence images of both Cy3 and NBD appeared homogeneous (not shown), indicative of no phase separation at the micrometer scale.

"Clumping" of the proteins due to their dissolution from the lipid matrix can be further detected by measuring FRET as a function of acceptor concentration. It has been shown that if the helices form dimers but no higher order aggregates (such that only monomers and dimers are present), FRET depends linearly on the acceptor ratio (*23*, *24*). Data shown in Figure 7 are indicative of a monomer−dimer equilibrium and no higher order aggregates.

Förster Resonance Energy Transfer (FRET). FRET experiments in vesicles were carried out using a Fluorolog fluorometer (Jobin Yvon). For Cy3/Cy5 samples, the excitation wavelength was set at 500 nm, and emission spectra were collected from 540 to 800 nm. For the Fl/Rhod donor/acceptor pair, the excitation wavelength was set at 439 nm, and emission spectra were collected from 450 to 800 nm. FRET was measured in liposomes containing known concentrations of donor- and acceptor-labeled proteins. Liposomes containing only donor-labeled proteins served as the "no FRET control". Energy transfer, *E*, was calculated from measurements of donor intensity at 568 nm (for Cy3/Cy5) or 519 nm (for Fl/Rhod) in the absence and presence of the acceptor.

$$E\,(\%) = (I_D - I_{DA})/(I_D) \times 100 \qquad (1)$$

where I_D and I_{DA} are the donor intensities of samples containing only donor-labeled proteins and samples with both donor- and acceptor-labeled proteins, respectively.

The Förster radii, R_0, for Fl/Rhod and Cy3/Cy5 are ∼55 Å. We expect that this value is a good estimate of R_0 in our FRET experiments because the dyes are attached to Cys396 close to the disordered C-terminus of the peptide (see above). Therefore the dyes should be positioned in the hydrated bilayer interface and be free to rotate.

To examine whether light scattering affects the fluorescence spectra, we carried out the described FRET experiments with unlabeled peptides and found that scattering is always negligible for wavelengths >450 nm.

Free Energy Calculations. We have found that the measured FRET signal depends only on the protein-to-lipid ratio (results not shown). It does not depend on the peptide and lipid concentrations of the samples, that is, on the amount of buffer added to hydrate the protein/lipid mixture. The mole fraction association constant, *K*, is therefore given by

$$K = [D]/[M]^2 \qquad (2)$$

where [D] is the dimer molar fraction in the lipid vesicles (dimers per lipid) and [M] is the monomer molar fraction in the lipid vesicles (monomers per lipid). The FRET efficiency (% FRET) is a measure of [D]/(2[D] + [M]). *K* is determined from a plot of FRET efficiency versus total peptide (per lipid) (Figure 10). The free energy of dimerization is given by

$$\Delta G = -RT \ln K \qquad (3)$$

RESULTS

SDS−PAGE. It has been shown that SDS−PAGE gels adequately report dimerization propensities of TM domain variants. In particular, changes in dimerization propensities due to amino acid substitutions, measured in bacterial membranes, have been shown to be the same in SDS detergent micelles. This has been demonstrated for the TM domain of GpA (*25*−*28*), as well as the TM domain of proapoptotic BNIP3 (Bcl-2 19 kDa interacting protein 3) (*29*). For both GpA and BNIP3, results from TOXCAT semiquantitative assays (which report dimerization in bacte-

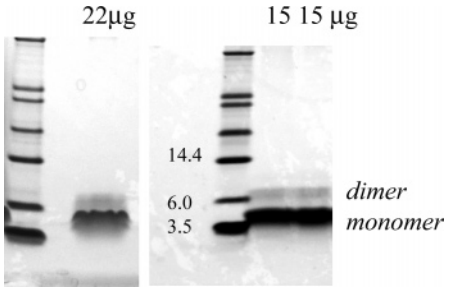

FIGURE 1: FGFR3 TM domain dimerizes in SDS micelles. Ten to thirty micrograms of peptide, dissolved in sample buffer, was reduced with NuPAGE reducing agent and boiled for 5 min prior to loading onto Novex precast tricine gels. The peptides were visualized with Coomassie blue. Two distinct bands, corresponding to the monomeric (3520.2 Da) and dimeric states, were observed. The left lanes show the molecular weight standards (molecular weight is in kDa). In more than 20 different SDS−PAGE experiments, we consistently observed between 5% and 10% dimer (calculated using the public domain NIH ImageJ software). The results shown are for 15 and 22 μg of peptide.

rial membranes) and from SDS−PAGE assays parallel one another. Thus, it appears that the dimer is stabilized by the same molecular interactions in membranes and in SDS micelles. The general validity of SDS−PAGE as an assay for TM helix dimerization is attributed to the fact that SDS does not disrupt all the TM domain dimers that form in the membrane, as demonstrated for phospholamban (*30*), β-barrel proteins (*31*), and the ammonium transporter AmtB (*32*). This is not surprising: while SDS is a denaturing environment for soluble proteins, SDS micelles mimic the bilayer environment and are therefore an adequate medium for probing TM helix dimerization. Now SDS−PAGE is routinely used to probe the occurrence of TM helix dimerization and the effect of a single amino acid substitution on dimer stability (*33*, *34*).

Using SDS−PAGE, we have investigated whether the FGFR3 TM domains dimerize in the absence of the extracellular domains and ligands. Typical SDS−PAGE results are shown in Figure 1. Two distinct bands, corresponding to monomers and dimers, were observed. The dimer−monomer ratios were calculated using the public domain NIH ImageJ software. In more than 20 different SDS−PAGE experiments, we consistently observed between 5% and 10% dimer. We therefore conclude that FGFR3 TM domain can dimerize in SDS in the absence of the extracellular domains and ligands. This finding is consistent with work from other laboratories, which has demonstrated that TM domains of other RTKs contribute to RTK dimer stabilization (*9*, *16*). However, FGFR3 TM domains do not dimerize as strongly as, for example, GpA: on a SDS gel, GpA runs as 100% dimer (*35*, *36*). The observed difference in dimerization is not surprising: while GpA is dimeric in the erythrocyte membrane, functional RTK TM domains should exist in a monomer/dimer equilibrium in the plasma membrane.

A major problem with long hydrophobic peptides is that they may aggregate and misfold, turning into β-sheet aggregates. We therefore asked whether the chemically synthesized TM domains are helical in SDS, such that the SDS−PAGE reports interactions between transmembrane helices. Figures 2 and 3 show the solution CD spectra of FGFR3 TM domains in various hydrophobic environments.

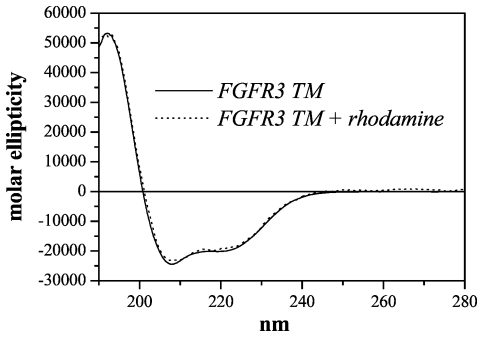

FIGURE 2: Effect of fluorescent dye conjugation on the solution CD spectra of FGFR3 TM domains in HFIP/TFE: (—) unlabeled FGFR3 TM domain; (•••) rhodamine-labeled FGFR3 TM domain. Helicities of unlabeled and labeled peptides are identical, suggesting that the attached label does not perturb the secondary structure of the peptide.

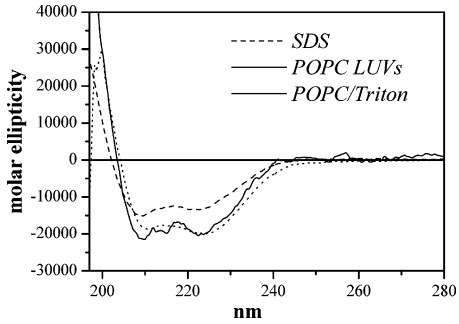

FIGURE 3: Solution CD spectra of FGFR3 TM domain in 4% (140 mM) SDS (− − −) and in lipid bilayer environments (POPC LUVs (—) and POPC/Triton (•••, see text for explanation). FGFR3 TM domain is helical in all hydrophobic environments.

The spectra show that the peptide is helical in all environments and in SDS in particular (Figure 3). Therefore, it appears that SDS−PAGE results report interaction between TM helices.

FRET in Liposomal Systems. FRET is widely used as a spectroscopic "ruler" for detecting molecular interactions in solution and in membranes. It involves the nonradiative transfer of energy from the excited state of a donor to an appropriate acceptor (*37*−*41*). If the two proteins dimerize, the donor and the acceptor will be brought in close contact such that FRET will occur. As a result, the donor fluorescence will decrease, and acceptor fluorescence will increase (*39*−*41*).

The efficiency of energy transfer, E, is inversely proportional to the sixth power of the distance, r, between the donor and acceptor. The transfer efficiency E is a function of r and R_0, the characteristic Förster radius for the donor and acceptor pair by

$$E = 1/[1 + (r/R_0)^6] \quad (4)$$

Typical donor/acceptor pairs, such as Cy3/Cy5 and Fl/Rhod, have R_0 of 50−60 Å. For this value of R_0 and $r = 10$−20 Å (typical for a helix dimer, helix diameter is 10 Å), E is 99%. For comparison, if $r = 100$ Å, E is negligible (1.5%). Therefore, dimerization causes a substantial energy transfer that can be easily detected.

In the present study, FRET was used to probe the dimerization of TM helices in POPC bilayers. The first task was to determine whether the dyes affect dimerization, and

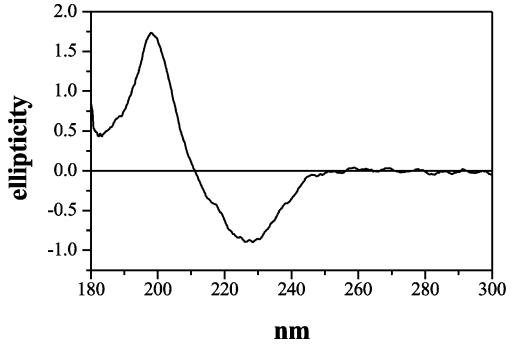

FIGURE 4: Oriented CD spectra of FGFR3 TM domain in oriented POPC bilayers. The samples were oriented multilayers on a quartz slide, deposited from an organic solvent. The multilayers were placed in the spectropolarimeter in such a way that they were normal to the optical path. The sample was rotated around the optical path in increments of 45°, and spectra were collected and averaged. This spectrum is indicative of a trasmembrane helix.

we therefore subjected the labeled and the unlabeled TM domains to SDS−PAGE. We could follow the colored bands of the labeled peptides, and we could observe monomer/dimer separation in real time. We then used Coomassie blue to stain all the peptides. For the labeled peptides, the Coomassie bands overlaid the colored bands (by visual inspection). The bands corresponding to labeled and unlabeled peptides appeared identical, suggesting that Cys396-attached fluorophores do not affect dimerization.

To determine whether the dyes affect the secondary structure of the TM domain, we measured the helicity of labeled and unlabeled peptides using circular dichroism (CD). Results, such as the ones shown in Figure 2, reveal that the dyes have no effect on helicity.

For measurements in liposomes one needs to further prove that the peptides are indeed transmembrane. To address this question, we collected CD spectra of FGFR3 TM domain in fully hydrated oriented POPC bilayers. The oriented CD spectrum is presented in Figure 4. The OCD spectra for helices that are normal and parallel to the bilayer plane are dramatically different (*19*, *20*, *42*). Helices that are parallel to the membrane plane exhibit two minima at 205 and 225 nm and a maximum around 192 nm. Transmembrane helices, however, exhibit a single minimum around 230 nm and a maximum around 200 nm. Therefore, the spectrum in Figure 4 is consistent with a transmembrane orientation of the helix. The position of the maximum at 200 nm, as well as the absence of a minimum at 205 nm suggests that the peptide is ∼100% transmembrane. In addition, the peptides are helical in POPC vesicles (see Figure 3).

We carried out FRET measurements using two different sets of FRET pairs: fluorescein/rhodamine (Fl/Rhod) and Cy3/Cy5. Figure 5 shows fluorescence spectra of Fl/Rhod-labeled peptides as a function of acceptor mole ratio. Spectra of samples containing Fl- and Rhod-labeled peptides (solid lines) are compared to the emission spectra of samples containing the same concentration of only Fl-labeled (dashed lines) and only Rhod-labeled (dotted lines) peptides.

Figure 6 shows FRET of Cy3/Cy5-labeled peptides as a function of peptide concentration. We show emission scans of LUVs containing both Cy3- and Cy5-labeled FGFR3 TM domain (solid lines), only Cy3-labeled FGFR3 TM domain (dashed lines), and only Cy5-labeled FGFR3 TM domain (dotted lines).

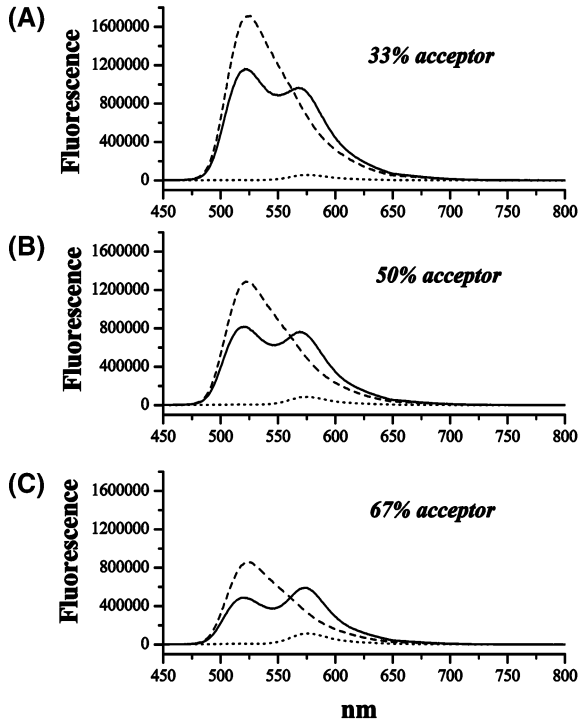

FIGURE 5: Fluorescence spectra of fluorescein/rhodamine-labeled peptides as a function of acceptor mole ratio: (A) 33% acceptor; (B) 50% acceptor; (C) 67% acceptor. Total peptide concentration was fixed at 0.2 mol %. Spectra were measured for samples containing fluorescein- (donor) and rhodamine-labeled (acceptor) peptides (—), as well as control samples containing only fluorescein-labeled (− − −) and only rhodamine-labeled peptides (···). In the experiments, Fl-labeled and Rhod-labeled peptides were premixed with lipids in organic solvent, the solvent was evaporated, and the samples were hydrated in buffer. After hydration, the samples were freeze−thawed three times to achieve full equilibration. The excitation was fixed at 439 nm such that only Fl was directly excited. The emission was scanned from 450 to 800 nm. FRET is obvious (—) from the decrease in Fl fluorescence (around 520 nm) and the appearance of sensitized Rhod fluorescence (around 570 nm). % FRET was calculated from the decrease in Fl fluorescence at 519 nm (eq 1).

In Figures 5 and 6, FRET is obvious from the decrease in donor fluorescence and the appearance of sensitized acceptor fluorescence. FRET, calculated as described in Materials and Methods, increases with increasing acceptor concentration at fixed total peptide concentration (see Figures 5 and 7). It also increases with increasing total peptide concentration for a fixed donor-to-acceptor ratio (Figures 6 and 10).

A question arises whether in the FRET experiments we probe the "correct" parallel dimer or some antiparallel, biologically irrelevant dimer. Ultimately, the answer to this question will come from structure determination. One concern may be that the positive charge "cluster" on the C-terminus interacts with the negative charge "cluster" on the N-terminus to form an antiparallel "loose" dimer. It has been shown that association in membranes, driven by electrostatics, depends on the salt concentration (*43*). We therefore reasoned that if this is the case, increasing the salt concentration will screen the electrostatic interactions and therefore decrease the observed FRET signal. We found that changes in salt concentration did not have an effect on FRET. This finding is preliminary evidence that electrostatic interactions do not play a crucial role in FGFR3 TM domain dimerization.

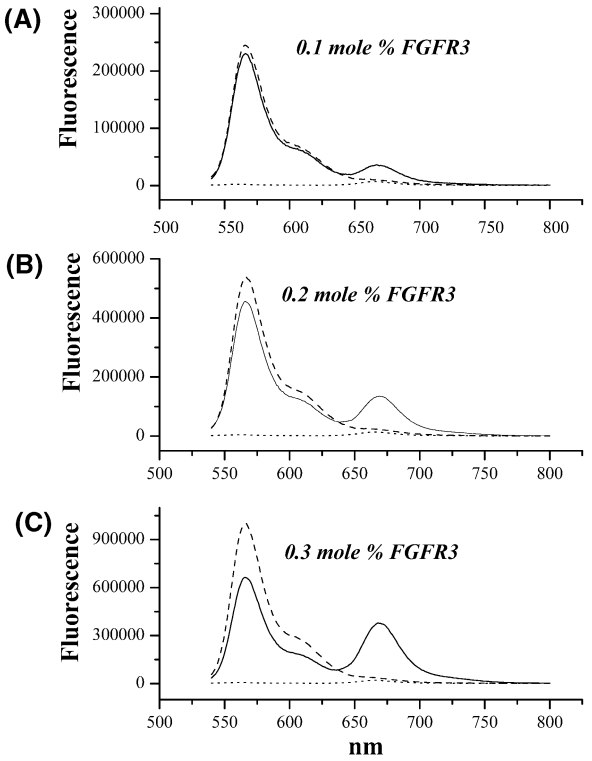

FIGURE 6: Fluorescence spectra of Cy3/Cy5-labeled peptides in extruded LUVs as a function of peptide concentration: (A) 0.1 mol % total peptide; (B) 0.2 mol % total peptide; (C) 0.3 mol % total peptide. The excitation was fixed at 450 nm such that only Cy3 was directly excited. The emission was scanned from 540 to 800 nm. Shown are (—) LUVs containing Cy3-labeled and Cy5-labeled FGFR3 TM domains, (– – –) LUVs containing Cy3-labeled FGFR3 TM domains, and (···) LUVs containing Cy5-labeled FGFR3 TM domains. FRET (—) results in decrease of Cy3 fluorescence (around 570 nm) and the appearance of sensitized Cy5 fluorescence (around 670 nm). FRET efficiencies were calculated from the decrease in Cy3 fluorescence at 568 nm (eq 1).

The FRET method relies on the assumption that highly homogeneous samples with proteins fully dissolved in the lipid matrix can be produced. As described in Materials and Methods, we assess sample homogeneity using various methods. For instance, protein aggregation due to protein/lipid phase separation can be detected by measuring FRET efficiencies in samples containing fixed protein concentration but different donor/acceptor ratios (as in Figure 5). It has been shown that if the helices form dimers but no higher order aggregates (such that only monomers and dimers are present), FRET depends linearly on the acceptor concentration (*23*, *24*). Figure 7 shows FRET as a function of acceptor concentration for Fl/Rhod-labeled peptides (A) and for Cy3/Cy5-labeled peptides (B). In these experiments, the peptide and lipid concentrations were kept constant, while the ratio of donor-labeled to acceptor-labeled peptides was varied. Percent energy transfer was calculated using eq 1 as described in Materials and Methods. The linear dependence of the energy transfer on the acceptor mole ratio in Figure 7 is indicative of monomer/dimer equilibrium and absence of higher order aggregates. The observed difference in slope is attributed to the different labeling yields for Fl/Rhod (Fl = 80%, Rhod = 100%) and Cy3/Cy5 (Cy3 = 34%, Cy5 = 54%) (see also Materials and Methods). The labeling yield does not affect the shape of the curve, provided that the same peptide stock is used for each measurement (*23*).

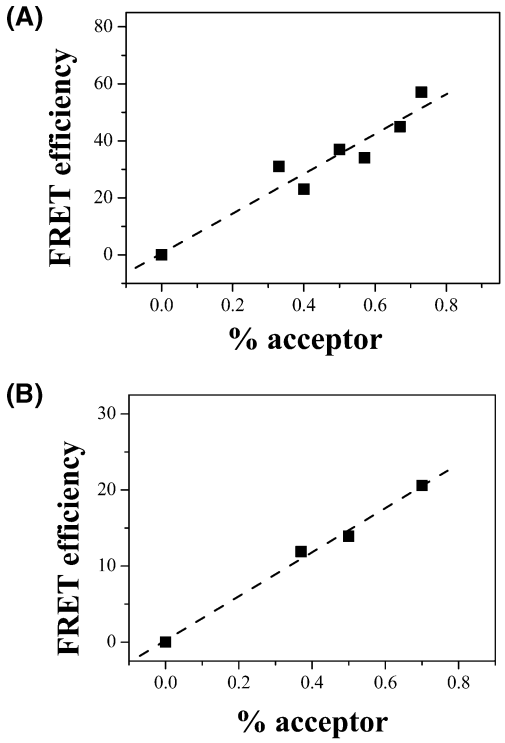

FIGURE 7: Energy transfer as a function of acceptor mole ratio: (A) results for fluorescein/rhodamine-labeled peptides (labeling yield for Fl = 80% and for Rhod = 100%); (B) results for Cy3/Cy5-labeled peptides (labeling yield for Cy3 = 34% and for Cy5 = 54%). FRET efficiencies were calculated using eq 1 as described in Materials and Methods. The peptide and lipid concentrations were kept constant, while the ratio of donor-labeled to acceptor-labeled peptides was varied. The linear dependence of the energy transfer on the acceptor mole ratio is indicative of dimer formation and absence of higher order aggregates.

Dimerization or Proximity Effects? FRET can arise simply due to proximity effects. In our experiments, we deliberately used low peptide concentration, never exceeding 0.15 mol % acceptor in the liposomes. We measured FRET efficiencies for peptide concentrations ranging from 1 peptide per 300 lipids to 1 peptide per 10 000 lipids. The average distances between the peptides under these conditions are between 150 and 840 Å, always exceeding the Förster radii for Fl/Rhod and Cy3/Cy5. However, the peptides diffuse in the bilayers, such that an acceptor can come in close contact with a donor, and FRET can occur. We therefore performed control experiments to determine whether the measured FRET signal is, in part, due to dimerization.

It has been shown that if dimerization occurs, the addition of unlabeled peptide to donor- and acceptor-labeled dimers will decrease the FRET signal. This control experiment has demonstrated that GpA forms sequence-specific dimers in SDS (*36*). Figure 8 shows the effect of adding unlabeled FGFR3 TM to the Rh/Fl-labeled dimers. Two liposomal solutions were prepared; both contained 0.1 mol % Fl-FGFR3 TM domain and 0.1 mol % Rhod-FGFR3 TM domain, and in addition to this, one of the samples (dashed line) contained also ~0.3 mol % unlabeled peptide. We see that FRET is reduced in the presence of the unlabeled peptide, indicative of dimerization. This result demonstrates that the observed FRET is not due to proximity effects only; sequence-specific dimerization also contributes to the measured FRET efficiency.

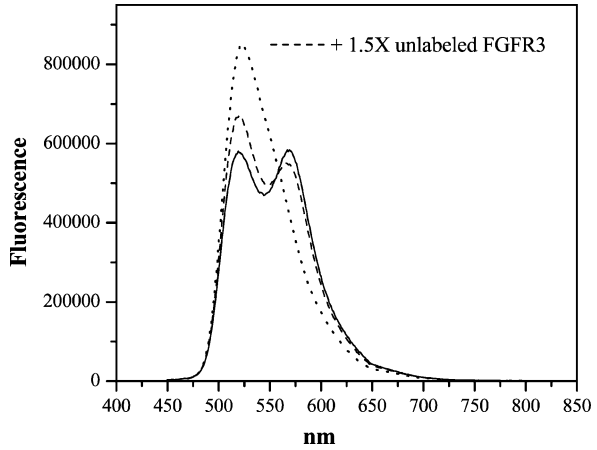

FIGURE 8: Addition of unlabeled FGFR3 TM domain reduces the FRET efficiency: (···) liposomes containing 0.1 mol % Fl-FGFR3 TM domain; (—) liposomes containing 0.1 mol % Fl-FGFR3 TM domain and 0.1 mol % Rhod-FGFR3 TM domain; (– – –) liposomes containing 0.1 mol % Fl-FGFR3 TM domain, 0.1 mol % Rhod-FGFR3 TM domain, and ~0.3 mol % unlabeled peptide. The reduced FRET efficiency in the presence of the unlabeled peptide suggests that sequence-specific dimerization contributes to the measured FRET efficiency.

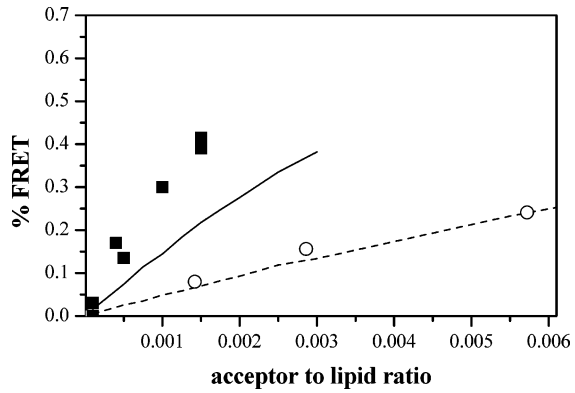

FIGURE 9: Effect of peptide proximity on measured FRET efficiencies. Curves computed according to the proximity analysis of Wolber and Hudson are shown for $R_0 = 30$ (– – –) and 55 Å (—). Also shown are data for tryptophan quenching by methylcoumarine with R_0 estimated to be around 25–30 Å (○, taken from ref *45*), as well as our data for Fl/Rhod-labeled FGFR3 TM domain (■). The solid squares deviate from the simulated theoretical curve, suggesting that both proximity effects and sequence-specific FGFR3 TM dimerization contribute to the observed FRET efficiency.

FRET efficiency due to proximity effects can be estimated computationally, as shown by Wolber and Hudson (*44*). FRET from randomly distributed peptides is calculated by averaging the donor quenching, q_i, by acceptors in a specific configuration over a large number of acceptor configurations. The quenching of a donor by a specific acceptor configuration is given by

$$q_i = [1 + \sum_i (R_0/R_i)^6]^{-1} \quad (5)$$

where R_i is the distance between the donor and an acceptor.

The calculation of proximity FRET as the average of 1000 different acceptor configurations is shown in Figure 9 for $R_0 = 30$ (dashed line) and 55 Å (solid line). The dashed line is compared to experimental data for tryptophan quenching by lysomethylcoumarine, published previously by Wimley and White (*45*). The R_0 of the tryptophan–methylcoumarin pair is estimated to be around 25–30 Å. There are no

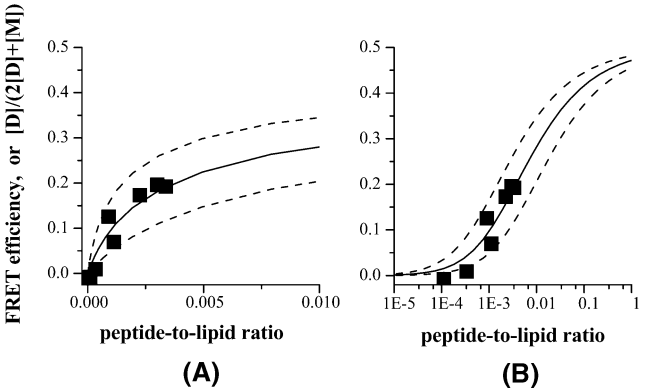

FIGURE 10: Energetics of FGFR3 TM domain dimerization in POPC vesicles. Fraction of dimer is shown as a function of total peptide concentration (plotted on a linear (A) and a logarithmic (B) scale). The dimer fraction is calculated from FRET efficiencies measured for Fl/Rhod-labeled peptides (labeling yield > 90%). Calculated FRET efficiencies due to proximity effects are subtracted from measured FRET to obtain FRET efficiencies due to dimerization. The solid line is calculated according to eq 2 with an association constant of 5.7×10^{-3}. This corresponds to dimerization free energy of approximately −3 kcal/mol. The dashed lines bracketing the data are calculated for $\Delta G = -3.5$ and $\Delta G = -2.5$ kcal/mol.

specific interactions between the tryptophan on the protein and the lysolipid, and the theory fits the experiment well. The solid curve for $R_0 = 55$ Å, a value reported for Fl/Rhod, however, substantially deviates from our experimental data, suggesting that proximity effects alone do not describe the observed FRET signal. As pointed out in Materials and Methods, $R_0 = 55$ Å should be a good estimate in our FRET experiments because the dyes are attached to Cys396 close to the disordered C-terminus of the peptide. Therefore the dyes should be positioned in the hydrated bilayer interface and be free to rotate (see below for additional arguments).

The result in Figure 9 further suggests that the observed FRET is partially due to dimerization and partially due to proximity effects. We therefore obtain the FRET efficiency due to dimerization by subtracting the predicted FRET efficiency due to proximity (solid line in Figure 9) from the measured FRET signal. Figure 10 shows the corrected FRET efficiency for Fl/Rhod-labeled peptides as a function of total peptide concentration (2[D] + [M]). The data shown were collected using peptides with high degree of labeling (>90% labeling). If the labeling yield was lower than a 100%, the results were corrected as described in Materials and Methods. The FRET efficiency is a measure of [D]/(2[D] + [M]) (0.5 × fraction of peptides in the dimeric state), where [D] is the dimer fraction in the lipid vesicles (dimers per lipid) and [M] is the monomer fraction in the lipid vesicles (monomers per lipid). The solid curve is calculated according to eq 2 with an association constant of 5.7×10^{-3}. This corresponds to a free energy of approximately −3 kcal/mol (see eq 3). Therefore, the presented FRET measurements suggest that the free energy of dimerization of FGFR3 TM domain is approximately −3 kcal/mol.

To illustrate the errors associated with the method, in Figure 10, we also show the theoretical curves for $\Delta G = -3.5$ and $\Delta G = -2.5$ kcal/mol (dashed lines). We see that the −3.5 and −2.5 kcal/mol curves bracket the data, which fall on the −3.0 kcal/mol line. Therefore, $\Delta G = -3.0 \pm 0.5$ kcal/mol.

It should be noted that changes in the free energy of dimerization shift the theoretical curve in Figure 10B to the right or to the left but do not change its slope. If the data are not corrected for proximity effects, the experimental slope deviates from the theoretically predicted one. The fact that the corrected experimental data (as given by the solid squares in Figure 10B) follow the theoretical slope (solid line in Figure 10B) suggests that the estimate for proximity effects, as given by the solid line in Figure 9, is reasonable. Therefore, the assumption for $R_0 = 55$ Å is also reasonable. A wrong assumption for R_0 will produce an experimental slope that deviates from the theoretical one in Figure 10B.

DISCUSSION

Do the TM Domains of RTKs Play a Crucial Role in RTK Signal Transduction? About a decade ago, the TM domains of RTKs were believed to simply anchor the proteins to the membrane (*8*), while the extracellular domains of RTKs participate in ligand recognition and drive the dimerization process (*5*−*7*). The first indication that the TM domains contain critical structural information that modulates receptor-mediated signal transduction was the finding that single amino acid substitutions in the TM domains can lead to constitutive receptor activation and therefore to pathologies (*1*, *10*, *11*). Recently, Mendrola et al. demonstrated that the TM domains of EGFR and the three other members of the ErbB family, ErbB2−4, dimerize in bacterial membranes (*16*). Work by Tanner and Kyte suggests that RTK TM domains may, in fact, be the driving force behind RTK dimerization (*9*). Work by Bell at al. (*46*) has demonstrated that RTK TM domains play yet another critical role in signal transduction: they position the kinase domains in the dimer in such a way that they can cross-phosphorylate each other. Correct orientation of the catalytic domains can be achieved only via the "correct" signaling-competent TM dimerization motif.

All the above findings suggest that the TM domains play an important role in the dimerization process. The SDS−PAGE and FRET results presented here show that FGFR3 TM domain dimerizes in the absence of the extracellular domain and ligand. However, dimerization propensity is low (−3 kcal/mol), when compared to the dimerization propensity of the only well-characterized TM dimer, GpA (less than −9 kcal/mol) (*36*, *47*).

This finding is not surprising: glycophorin A is a stable dimer in the erythrocyte membrane, while RTKs conduct signals via lateral dimerization. It is easy to envision that control over RTK-mediated signal transduction across the plasma membrane will be impossible to achieve if the dimerization propensity is strong. Weak dimerization, on the other hand, should allow for a tight control over the monomer/dimer equilibrium. Therefore, low dimerization propensity may be expected for all RTK TM domains, a hypothesis that remains to be verified.

FGFR3 TM Domain and Human Pathologies. FGFR3 is critical for embryogenesis, angiogenesis, and tissue repair (*48*−*50*). Mutations in the FGFR3 gene underlie dominant disorders of bone development, such as achondroplasia, thanatophoric dysplasia types 1 and 2, hypochondroplasia, and Crouzon syndrome with acanthosis nigricans (*17*, *51*), as well as epithelium cancers (*13*). Several of these mutations appear in the TM domain of the receptor. It has been proposed that these pathogenic FGFR3 TM domain mutations cause unregulated signaling by stabilizing the mutant dimers. While the dimerization energetics of the mutant proteins is yet to be worked out, the results presented in this paper provide a starting point for understanding the thermodynamic consequences of these mutations. The weak dimerization propensity measured here suggests that if a mutation increases the dimerization free energy by only a few kilocalories per mole, it may still result in substantial changes in monomer/dimer distributions and dramatic effect on signaling.

ACKNOWLEDGMENT

We are grateful to Dr. William Wimley for many valuable discussions. We thank Drs. John Tomich and Takeo Iwamoto for peptide synthesis, and Drs. Wimley and A. K. Kenworthy for reading the manuscript prior to publication. We acknowledge Jamie Chou's help with the FRET experiments.

REFERENCES

1. Hynes, N. E., and Stern, D. F. (1994) The biology of *erbB*-2/*neu*/*HER*-2 and its role in cancer, *Biochim. Biophys. Acta 1198*, 165−184.
2. Cappellen, D., de Oliveira, C., Ricol, D., Diez de Medina, S. G., Bourdin, J., Sastre-Garau, X., Chopin, D., Thiery, J. P., and Radvanyi, F. (1999) Frequent activating mutations of FGFR3 in human bladder and cervix carcinomas, *Nat. Genet. 23*, 18−20.
3. Wilkie, A. O. M., Morriss-Kay, G. M., Jones, E. Y., and Heath, J. K. (1995) Functions of fibroblast growth factors and their receptors, *Curr. Biol. 5*, 500−507.
4. Schlessinger, J. (2002) Ligand-induced, receptor-mediated dimerization and activation of EGF receptor, *Cell 110*, 669−672.
5. Lemmon, M. A., Bu, Z. M., Ladbury, J. E., Zhou, M., Pinchasi, D., Lax, I., Engelman, D. M., and Schlessinger, J. (1997) Two EGF molecules contribute additively to stabilization of the EGFR dimer, *EMBO J. 16*, 281−294.
6. Spivakkroizman, T., Lemmon, M. A., Dikic, I., Ladbury, J. E., Pinchasi, D., Huang, J., Jaye, M., Crumley, G., Schlessinger, J., and Lax, I. (1994) Heparin-Induced Oligomerization of Fgf Molecules Is Responsible for Fgf Receptor Dimerization, Activation, and Cell-Proliferation, *Cell 79*, 1015−1024.
7. Lemmon, M. A., and Schlessinger, J. (1994) Regulation of Signal-Transduction and Signal Diversity by Receptor Oligomerization, *Trends Biochem. Sci. 19*, 459−463.
8. Lemmon, M. A., and Engelman, D. M. (1994) Specificity and promiscuity in membrane helix interactions, *Q. Rev. Biophys. 27*, 157−218.
9. Tanner, K. G., and Kyte, J. (1999) Dimerization of the extracellular domain of the receptor for epidermal growth factor containing the membrane-spanning segment in response to treatment with epidermal growth factor, *J. Biol. Chem. 274*, 35985−35990.
10. Miloso, M., Mazzotti, M., Vass, W. C., and Beguinot, L. (1995) SHC and GRB-2 are constitutively activated by an epidermal growth factor receptor with a point mutation in the transmembrane domain, *J. Biol. Chem. 270*, 19557−19562.
11. Bange, J., Prechtl, D., Cheburkin, Y., Specht, K., Harbeck, N., Schmitt, M., Knyazeva, T., Muller, S., Gartner, S., Sures, I., Wang, H. Y., Imyanitov, E., Haring, H. U., Knayzev, P., Iacobelli, S., Hofler, H., and Ullrich, A. (2002) Cancer progression and tumor cell motility are associated with the FGFR4 Arg(388) allele, *Cancer Res. 62*, 840−847.
12. Meyers, G. A., Orlow, S. J., Munro, I. R., Przylepa, K. A., and Jabs, E. W. (1995) Fibroblast-Growth-Factor-Receptor-3 (Fgfr3) Transmembrane Mutation in Crouzon-Syndrome with Acanthosis Nigricans, *Nat. Genet. 11*, 462−464.
13. van Rhijin, B., van Tilborg, A., Lurkin, I., Bonaventure, J., de Vries, A., Thiery, J. P., van der Kwast, T. H., Zwarthoff, E., and Radvanyi, F. (2002) Novel fibroblast growth factor receptor 3 (FGFR3) mutations in bladder cancer previously identified in nonlethal skeletal disorders, *Eur. J. Hum. Genet. 10*, 819−824.

14. Shiang, R., Thompson, L. M., Zhu, Y.-Z., Church, D. M., Fielder, T. J., Bocian, M., Winokur, S. T., and Wasmuth, J. J. (1994) Mutations in the transmembrane domain of FGFR3 cause the most common genetic form of dwarfism, achondroplasia, *Cell 78*, 335−342.
15. Segatto, O., King, C. R., Pierce, J. H., di Fiore, P. P., and Aaronson, S. A. (1988) Different structural alterations upregulate in vitro tyrosine kinase activity and transforming potency of the *erbB*-2 gene, *Mol. Cell. Biol. 8*, 5570−5574.
16. Mendrola, J. M., Berger, M. B., King, M. C., and Lemmon, M. A. (2002) The single transmembrane domains of ErbB receptors self-associate in cell membranes, *J. Biol. Chem. 277*, 4704−4712.
17. Vajo, Z., Francomano, C. A., and Wilkin, D. J. (2000) The molecular and genetic basis of fibroblast growth factor receptor 3 disorders: The achondroplasia family of skeletal dysplasias, Muenke craniosynostosis, and Crouzon syndrome with acanthosis nigricans, *Endocr. Rev. 21*, 23−39.
18. Webster, M. K., and Donoghue, D. J. (1996) Constitutive activation of fibroblast growth factor receptor 3 by the transmembrane domain point mutation found in achondroplasia, *EMBO J. 15*, 520−527.
19. Olah, G. A., and Huang, H. W. (1988) Circular dichroism of oriented α helices. I. Proof of the exciton theory, *J. Chem. Phys. 89*, 2531−2538.
20. Olah, G. A., and Huang, H. W. (1988) Circular dichroism of oriented α helices. II. Electric field oriented polypeptides, *J. Chem. Phys. 89*, 6956−6962.
21. Hristova, K., Wimley, W. C., Mishra, V. K., Anantharamaiah, G. M., Segrest, J. P., and White, S. H. (1999) An amphipathic α-helix at a membrane interface: A structural study using a novel X-ray diffraction method, *J. Mol. Biol. 290*, 99−117.
22. Hristova, K., Dempsey, C. E., and White, S. H. (2001) Structure, location, and lipid perturbations of melittin at the membrane interface, *Biophys. J. 80*, 801−811.
23. Adair, B. D., and Engelman, D. M. (1994) Glycophorin a helical transmembrane domains dimerize in phospholipid bilayers − a resonance energy transfer study, *Biochemistry 33*, 5539−5544.
24. Li, M., Reddy, L. G., Bennett, R., Silva, N. D., Jones, L. R., and Thomas, D. D. (1999) A fluorescence energy transfer method for analyzing protein oligomeric structure: Application to phospholamban, *Biophys. J. 76*, 2587−2599.
25. Lemmon, M. A., Flanagan, J. M., Hunt, J. F., Adair, B. D., Bormann, B. J., Dempsey, C. E., and Engelman, D. M. (1992) Glycophorin-A dimerization is driven by specific interactions between transmembrane α-helices, *J. Biol. Chem. 267*, 7683−7689.
26. Lemmon, M. A., Flanagan, J. M., Hunt, J. F., Adair, B. D., Bormann, B. J., Dempsey, C. E., and Engelman, D. M. (1992) Glycophorin-A Dimerization Is Driven by Specific Interactions Between Transmembrane Alpha-Helices, *J. Biol. Chem. 267*, 7683−7689.
27. Russ, W. P., and Engelman, D. M. (1999) TOXCAT: A measure of transmembrane helix association in a biological membrane, *Proc. Natl. Acad. Sci. U.S.A. 96*, 863−868.
28. Fleming, K. G., and Engelman, D. M. (2001) Specificity in transmembrane helix-helix interactions can define a hierarchy of stability for sequence variants, *Proc. Natl. Acad. Sci. U.S.A. 98*, 14340−14344.
29. Sulistijo, E. S., Jaszewski, T. M., and MacKenzie, K. R. (2003) Sequence-specific dimerization of the transmembrane domain of the "BH3-only" protein BNIP3 in membranes and detergent, *J. Biol. Chem. 278*, 51950−51956.
30. Cornea, R. L., Jones, L. R., Autry, J. M., and Thomas, D. D. (1997) Mutation and phosphorylation change the oligomeric structure of phospholamban in lipid bilayers, *Biochemistry 36*, 2960−2967.
31. Watanabe, Y. (2002) Effect of various mild surfactants on the reassembly of an oligomeric integral membrane protein OmpF porin, *J. Protein Chem. 21*, 169−175.
32. Blakey, D., Leech, A., Thomas, G. H., Coutts, G., Findlay, K., and Merrick, M. (2002) Purification of the *Escherichia coli* ammonium transporter AmtB reveals a trimeric stoichiometry, *Biochem. J. 364*, 527−535.
33. Partridge, A. W., Melnyk, R. A., and Deber, C. M. (2002) Polar residues in membrane domains of proteins: Molecular basis for helix-helix association in a mutant CFTR transmembrane segment, *Biochemistry 41*, 3647−3653.
34. Melnyk, R. A., Partridge, A. W., and Deber, C. M. (2002) Transmembrane domain mediated self-assembly of major coat protein subunits from Ff bacteriophage, *J. Mol. Biol. 315*, 63−72.
35. Melnyk, R. A., Partridge, A. W., and Deber, C. M. (2001) Retention of native-like oligomerization states in transmembrane segment peptides: Application to the *Escherichi coli* aspartate receptor, *Biochemistry 40*, 11106−11113.
36. Fisher, L. E., Engelman, D. M., and Sturgis, J. N. (1999) Detergents modulate dimerization, but not helicity, of the glycophorin A transmembrane domain, *J. Mol. Biol. 293*, 639−651.
37. Wu, P., and Brand, L. (1994) Resonance energy transfer: Methods and applications, *Anal. Biochem. 218*, 1−13.
38. Kenworthy, A. K., Petranova, N., and Edidin, M. (2000) High-resolution FRET microscopy of cholera toxin B-subunit and GPI-anchored proteins in cell plasma membranes, *Mol. Biol. Cell 11*, 1645−1655.
39. Kenworthy, A. K., and Edidin, M. (1998) Distribution of a glycosylphosphatidylinositol-anchored protein at the apical surface of MDCK cells examined at a resolution of <100 Å using imaging fluorescence resonance energy tranfer, *J. Cell Biol. 142*, 69−84.
40. Clegg, R. M. (1995) Fluorescence resonance energy transfer, *Curr. Opin. Biotechnol. 6*, 103−110.
41. Clegg, R. M. (1996) in *Fluorescence Imaging Spectroscopy and Microscopy* (Wang, X. F. and Herman, B., Eds.) pp 179−252, John Wiley, New York.
42. Wu, Y., Huang, H. W., and Olah, G. A. (1990) Method of oriented circular dichroism, *Biophys. J. 57*, 797−806.
43. Gambhir, A., Hangyas-Mihalyne, G., Zaitseva, I., Cafiso, D. S., Wang, J. Y., Murray, D., Pentyala, S. N., Smith, S. O., and McLaughlin, S. (2004) Electrostatic sequestration of PIP2 on phospholipid membranes by basic/aromatic regions of proteins, *Biophys. J. 86*, 2188−2207.
44. Wolber, P. K., and Hudson, B. S. (1979) An analytic solution to the Förster energy transfer problem in two dimensions, *Biophys. J. 28*, 197−210.
45. Wimley, W. C., and White, S. H. (2000) Determining the membrane topology of peptides by fluorescence quenching, *Biochemistry 39*, 161−170.
46. Bell, C. A., Tynan, J. A., Hart, K. C., Meyer, A. N., Robertson, S. C., and Donoghue, D. J. (2000) Rotational coupling of the transmembrane and kinase domains of the Neu receptor tyrosine kinase, *Mol. Biol. Cell 11*, 3589−3599.
47. Fleming, K. G., Ackerman, A. L., and Engelman, D. M. (1997) The effect of point mutations on the free energy of transmembrane α-helix dimerization, *J. Mol. Biol. 272*, 266−275.
48. Deng, C., Wynshaw-Boris, A., Zhou, F., Kuo, A., and Leder, P. (1996) Fibroblast growth factor receptor 3 is a negative regulator of bone growth, *Cell 84*, 911−921.
49. Nguyen, H. B., Estacion, M., and Gargus, J. J. (1997) Mutations causing achondroplasia and thanatophoric dysplasia alter bFGF-induced calcium signals in human diploid fibroblasts, *Hum. Mol. Genet. 6*, 681−688.
50. Colvin, J. S., Bohne, B. A., Harding, G. W., Mcewen, D. G., and Ornitz, D. M. (1996) Skeletal overgrowth and deafness in mice lacking fibroblast growth factor receptor 3, *Nat. Genet. 12*, 390−397.
51. Passos-Bueno, M. R., Wilcox, W. R., Jabs, E. W., Sertié, A. L., Alonso, L. G., and Kitoh, H. (1999) Clinical spectrum of fibroblast growth factor receptor mutations, *Hum. Mutat. 14*, 115−125.

BI048480K